Chin. Phys. Lett. **39**, 036101 (2022) **Express Letter**

High Energy Density Polymeric Nitrogen Nanotubes inside Carbon Nanotubes

Chi Ding(丁驰), Junjie Wang(王俊杰), Yu Han(韩瑜), Jianan Yuan(袁嘉男), Hao Gao(高豪), and Jian Sun(孙建)*

National Laboratory of Solid State Microstructures, School of Physics and Collaborative Innovation Center of Advanced Microstructures, Nanjing University, Nanjing 210093, China

(Received 22 December 2021; accepted 28 January 2022; published online 3 February 2022)

Polymeric nitrogen as a new class of high energy density materials has promising applications. We develop a new scheme of crystal structure searching in a confined space using external confining potentials fitted from first-principles calculations. As a showcase, this method is employed to systematically explore novel polymeric nitrogen structures confined in single-walled carbon nanotubes. Several quasi-one-dimensional single-bonded polymeric nitrogen structures are realized, two of them are composed of nanotubes instead of chains. These new polymeric nitrogen phases are mechanically stable at ambient pressure and temperature according to phonon calculations and *ab initio* molecular dynamics simulations. It is revealed that the stabilization of zigzag and armchair chains confined in carbon nanotubes are mostly attributed to the charge transfer from carbon to nitrogen. However, for the novel nitrogen nanotube systems, electrons overlapping in the middle space provide strong Coulomb repulsive forces, which not only induce charge transfer from the middle to the sides but also stabilize the polymeric nitrogen. Our work provides a new strategy for designing novel high-energy-density polymeric nitrogen materials, as well as other new materials with the help of confined space inside porous systems, such as nanotubes, covalent organic frameworks, and zeolites.

DOI: 10.1088/0256-307X/39/3/036101

Polymeric nitrogen has attracted increasing attention due to their potential applications as high energy density materials (HEDMs).[1–9] Because the bond energy of N≡N triple bond (954 kJ/mol) is several times larger than that of the N–N single bond (160 kJ/mol) and N=N double bond (418 kJ/mol), a huge amount of energy will be released when polymeric nitrogen bonded with single and/or double bonds is decomposed into isolated nitrogen molecules.[7,10] Therefore, polymeric nitrogen can be used as explosives or propellants.[11] Moreover, nitrogen gas as the final product of the above-mentioned chemical reaction is inert and stable so that it has a small influence on the environment. With these alluring properties, several phases of polymeric nitrogen have been predicted theoretically, including the cubic-gauge nitrogen (cg-N),[1] layered *Pba*2 phase,[3] cage-like diamondoid nitrogen,[5] and metallic salt,[6] etc. In 2004, the cg-N was firstly reported to be synthesized under high pressure of 110 GPa over 2000 K.[2] Since then, several other polymeric structures have been experimentally obtained using high-pressure methods.[7–9,12,13] Unfortunately, none of these polymeric nitrogen phases have been quenched to ambient conditions in experiments up to now. For a long time, researchers have been devoted to quenching polymeric nitrogen to lower pressure. To use the chemical pressure as a solution, some nitrogen-rich compounds containing polymeric nitrogen units, such as N_4 unit, N_5, N_6 rings, or polymeric chains have been proposed and synthesized,[14–26] some of them are even stable under ambient conditions. In this Letter, we propose that strong confining potentials may be another efficient approach to obtaining pure polymeric nitrogen at relatively low pressure.

The confined space inside carbon nanotubes (CNTs) has been used as a "reaction chamber" to synthesize nano structures.[27–30] CNTs not only provide a natural space for atoms or molecules to fill[31,32] but also protect them from oxidization and help to stabilize those structures that may not exist in a vacuum space or one-dimensional form stand-alone.[33,34] More importantly, the carbon networks are strong enough so that they can provide a proper confining potential. Therefore, carbon nanotubes may be excellent containers for accommodation of polymeric nitrogen. Two polymeric nitrogen structures, the zigzag and armchair N8 chain,[35,36] have been predicted to be stable when confined in carbon nanotubes under ambient conditions. However, nitrogen atoms in these two phases are twofold-coordinated so that the bond lengths are between those of typical single and double

*Corresponding author. Email: jiansun@nju.edu.cn
© 2022 Chinese Physical Society and IOP Publishing Ltd

bonds, thus there is still a large potential energy density that can be explored. Recently, an interesting experimental work shows that cg-N can be synthesized with the help of carbon nanotubes,[37] 100-nm-long multi-wall nanotubes were dispersed with β-sodium azide, and then the plasma flow of the mixture of nitrogen and argon was introduced into the deposition chamber for 2 h. After that, the cubic gauge nitrogen was synthesized within CNTs. The above-mentioned work demonstrated the possibility to realize complex nitrogen networks under ambient conditions. However, in most of the previous works, researchers only put known polymeric nitrogen structures into CNTs and then check their stability.[38–40] A more systematic crystal structure searching inside a confined space is still missing, and it is still unknown whether there are other polymeric nitrogen networks with a higher energy density that can be achieved in carbon nanotubes.

In this work, we develop a new scheme of crystal structure searching in a confined space combining the machine learning accelerated crystal structure search method (Magus)[41] together with external confining potentials fitted from first-principles calculations. As a showcase, this scheme is employed to systematically explore novel polymeric nitrogen phases confined in single-walled carbon nanotubes (SWCNTs). We identify several novel nitrogen structures with single-bonded networks inside SWCNTs of different sizes. Moreover, when encapsulated into practical carbon nanotubes, all of them can retain the chain-like or tube-like polymers without decomposing into N_2 molecules. The size effects of carbon nanotubes and the stabilization mechanism of these polymeric nitrogen structures inside CNTs are carefully discussed. Most importantly, these combined systems with the tube-like nitrogen polymer possess a very large energy density, which is almost twice that of trinitrotoluene (TNT), indicating their striking applications.

Results—Crystal Structure Predictions. To demonstrate this work intuitively, we exhibit the flow chart of the crystal structure prediction in a confined space in Fig. 1(a). During structure searching, we introduced several cylindrical confining potentials called implicit carbon nanotubes (ICNTs)[27] as plotted in Fig. 1(b). These ICNTs not only reduce the computational cost but also help to solve the problem of the lattice mismatch between the polymeric nitrogen and carbon nanotubes along the c axis. These ICNTs were well fitted from the *ab initio* interaction potentials between CNTs and a nitrogen molecule. The obtained interaction forces are strongly repulsive, and their strength increases dramatically with reducing the distance from the nitrogen to the CNTs. With the increasing size of CNTs, the confined space in ICNTs expands and a relatively flat confining potential appears in the center. The attractive double-well potentials only appear in large sizes of CNTs [$(n, 0)$ with $n \geq 11$ and (n, n) with $n \geq 6$]. Polymeric nitrogen structure seeds were generated randomly and one example of these seeds is shown in Fig. 1(c), it is periodic along the c axis.

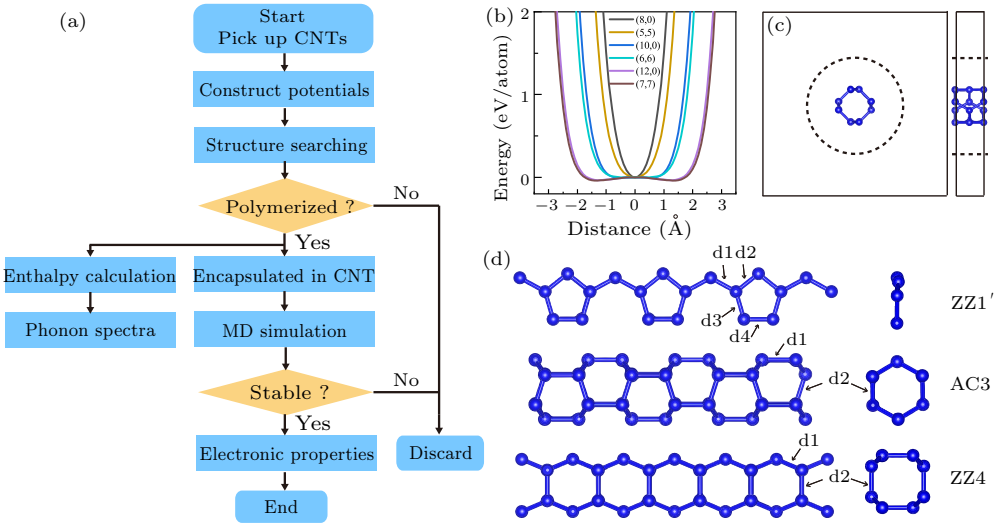

Fig. 1. (a) Illustration of the flow chart of crystal structure prediction inside a confined space. (b) The confining potentials of different implicit carbon nanotubes (ICNTs) applied on nitrogen molecule fitted from first-principles calculations. The horizontal coordinates represent the distance from the nitrogen atom to the center of carbon nanotubes. (c) One explicit example of the structures used for *ab initio* calculations, the dashed lines representing the position of the carbon nanotube or the border of the corresponding ICNT. (d) The top and side views of the three novel polymeric nitrogen structures predicted in this work. Different bonds in these structures are labeled.

Globally, we employed the evolutionary algorithm to search for the candidate structures. We performed the fixed-composition evolutionary algorithm for 20 generations, with 30 populations in each generation. The initial population was constructed with specified space groups. Moreover, 30% of the parent populations with lower energies were used to generate the child population and the heredity and special coordination mutations were employed. We optimized every candidate structure by fixing the lattice constants a and b while releasing the lattice constants c. The cell shapes maintain tetragonal during the optimization. The atomic positions were optimized to the energy local minimum. Due to the strong confinement of the ICNTs as shown in Fig. 1(c), the nitrogen atoms keep staying in the middle region of the cell. In addition to the previously known armchair and zigzag N8 chains,[35,36] here we found three different polymeric nitrogen phases within the $(n, 0)$ ICNTs (n = 8–12), as shown in Fig. 1(d). We named these newly identified phases as ZZ1′, AC3, and ZZ4, respectively, according to the type and number of chain polymer. Take the ZZ1′ as an example, ZZ1 means that the structure was mostly composed of one zigzag chain, the apostrophe in the upper right represents extra nitrogen atoms besides the chain. By the way, this structure can also be viewed as a chain of N_5 rings linked by nitrogen atoms. There are four different bonds in ZZ1′, i.e., d1, d2, d3, and d4, as denoted in Fig. 1(d). As for AC3, there are three armchair chains covalently bonded with each other, by this, they form a hexagonal nanotube. There are two different bonds in this structure as denoted with d1 and d2. As for ZZ4, it was composed of four zigzag chains, which results in a truncated square nanotube structure. In this phase, d1 represents the bond within the zigzag chain and d2 represents the bond between different chains. It is evident that the diameters of these quasi-1D polymeric structures are positively related to the number of chains. Except for the nitrogen phases mentioned above, there are several other more complicated types of structures identified in our structure searching or AIMD simulations as displayed in Fig. S2.

Enthalpy Calculation. The enthalpies of these newly identified polymeric nitrogen phases together with the previously studied N8 chains were calculated as a function of vertical pressure in the range of 0–10 GPa. The vertical pressure P_v is defined as the uniaxial stress σ_{zz} applied on the nitrogen tubes along the direction of z. Considering the cylindrical configuration of the carbon nanotubes, the confined space is also cylindrical, and the confinement is only limited to the direction of x and y, the confinement along the direction of z is absent. Thus, to get these polymeric nitrogen structures, we need to employ the uniaxial stress on the polymeric nitrogen. Two typical confining environments (9,0) and (10,0) ICNTs were employed, which exhibit very different results as shown in Fig. 2 due to different diameters.

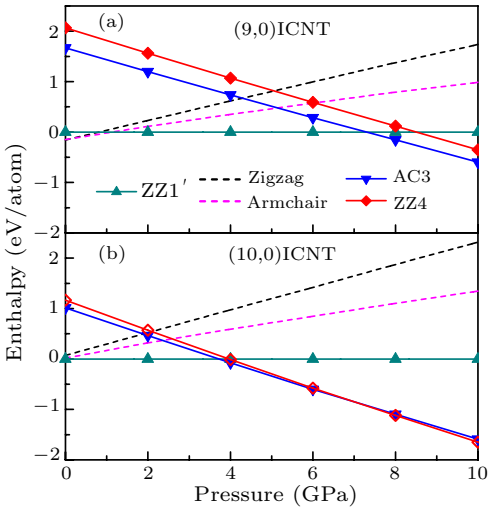

Fig. 2. Enthalpies of the polymeric nitrogen structures as a function of uniaxial stress σ_{zz} with (9,0) and (10,0) ICNT confining potentials. The diameters of practical (9,0) and (10,0) CNTs are 7.05 and 7.83 Å, respectively. Enthalpies are calculated with $H = E_{\text{nitrogen}} + E_{\text{confinement}} + P_v \times A \times L$, where E_{nitrogen} represents the total internal energy per nitrogen atom, $E_{\text{confinement}}$ coming from the confining potential of ICNT. P_v, A, and L represent the uniaxial stress σ_{zz}, bottom surface area of corresponding CNT bundles, and the length of cells in the c axis, respectively. All the enthalpy results are plotted relative to that of the ZZ1′ phase.

In addition, the results within (8,0) and (5,5) ICNTs are plotted in Fig. S3. When confined in the (9,0) ICNT, the zigzag and armchair chains are the most favorable phases at ambient pressure, whereas they will evolve into the ZZ1′ phase when applied with a mild pressure. Upon the increase of vertical pressure, single chains are not able to maintain their stability, several parallel chains will be joined together to form a quasi-1D nitrogen nanotube to stabilize the polymeric structure. For example, the single-chain polymer ZZ1′ will be replaced energetically by the nanotube phase AC3 at approximately 7.5 GPa. When confined in the (10,0) ICNT, these chain polymer phases, i.e., armchair, zigzag, and ZZ1′, have very similar enthalpies at zero vertical pressure. However, as applying pressure, ZZ1′ will transform into AC3 at a much lower pressure (about 4 GPa) than in the (9,0) ICNT. Because the confined space in the (9,0) ICNT is very narrow, the corresponding implicit confining potential applied on ZZ4 is much stronger than on AC3, therefore the enthalpy of the former is always ∼0.4 eV/atom higher than the latter in the whole pressure range. However, when confined in a much wider space such as the (10,0) ICNT, the interaction potentials employed on these two phases turn to be close and their enthalpy

difference is small. A vertical pressure of about 7 GPa will make the AC3 transform into ZZ4 in the (10,0) ICNT. Thus, the size of confining potentials is very essential to the energetic stability of the guest polymeric nitrogen and an appropriate size of carbon nanotube should be necessary for the experimental synthesis of these novel nitrogen phases.

Phonon Spectrum and Dynamical Stability. To explore the dynamical stability of polymeric nitrogen, we calculated the phonon dispersion curves of these three newly predicted phases (ZZ1′@(9,0)ICNT, AC3@(5,5)ICNT, and ZZ4@(10,0)ICNT) at zero vertical pressure as shown in Fig. S4. Due to the one-dimensional form of these phases, there is only one translational symmetry along the c axis. However, there is an additional rotation symmetry owing to the cylindrical confining potentials. Thus, we can see two acoustic branches across zero frequency at the gamma point. No imaginary phonon frequencies are found in the whole Brillouin zone for AC3 and ZZ4, indicating their mechanical stability. However, there is a small imaginary frequency appearing in the acoustic branch for ZZ1′@(9,0) ICNT, indicating a twist of this phase. When confined in a much stronger external potential such as in (8,0) ICNT, the imaginary frequency disappears. The above results emphasize the importance of the size of CNTs on the stability of the confined polymeric nitrogen again, an appropriate repulsive confining potential is necessary and sufficient to stabilize the polymeric nitrogen.

Stability in Practical CNTs. To explore the properties of these nitrogen phases in a real environment, we further encapsulated them into practical carbon nanotubes instead of ICNT potentials. Due to the incommensurability between CNTs and polymeric nitrogen units, special sizes of supercells were created to meet the commensurability conditions (the ratio of nitrogen and CNT elementary units was set as 1 : 1, 2 : 3 and 2 : 1 for ZZ1′@$(n,0)$CNT, AC3@(n,n)CNT and ZZ4@$(n,0)$CNT, respectively). Moreover, a special value of c length was chosen so that the vertical pressure applied on the nitrogen polymer was zero. As same as in the ICNT systems, a vacuum space larger than 10 Å between adjacent CNTs was employed. The final obtained structure parameters of these phases are displayed in Tables S2 and S3.

As can be seen in Table S2, the lengths of these four different bonds in ZZ1′ are very similar to each other, the average bond length at (9,0) CNT is 1.33 Å, which is in the range of N–N single bond (∼1.45 Å) and N=N double bond (∼1.25 Å). With the increase of CNT's size, these bonds have a very weak expansion. The most significant change occurs in the d3 bond, which stretches from ∼1.318 Å to ∼1.353 Å, representing the expansion of the distance from the main zigzag chain to the additional nitrogen atom. Because the structure of ZZ1′ is very anisotropic along the a and b directions, the cross section of the carbon nanotube will deform into an ellipse shape as shown in Fig. 3(a). As a result, this kind of deformation may help stabilize the ZZ1′ chain that prevents it from twisting as mentioned before. Table S2 shows the semi-major and semi-minor axis of the fully optimized elliptical carbon nanotubes when encapsulated with polymeric nitrogen. Their difference is large at a small size of (8,0) CNT (around 19.9%). However, with the increasing size of CNTs, their lengths come close to each other that the difference reaches approximately zero at (12,0) CNT (around 0.2%). Such weak anisotropic deformation cannot prevent the polymeric ZZ1′ from twisting as proved in our AIMD simulations.

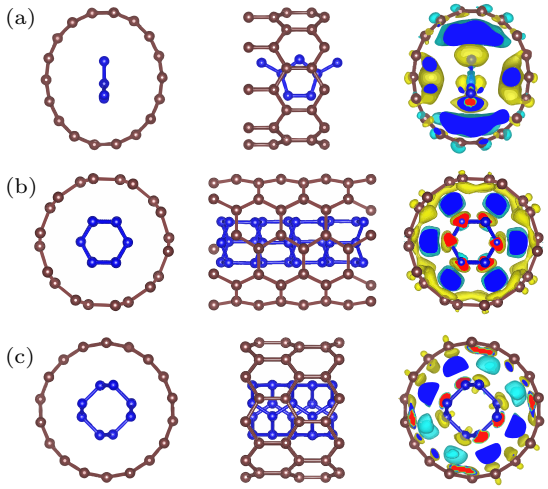

Fig. 3. Top and side views of structures of the three combined systems: ZZ1′@(9,0)CNT, AC3@(5,5)CNT and ZZ4@(9,0)CNT after geometry optimization, and the charge density difference between the combined systems and the sum of stand-alone nitrogen and carbon nanotube with the isosurface values 0.3×10^{-3}, 1.6×10^{-3} and 1.7×10^{-3}, respectively.

As to the polymeric ZZ4 nanotube systems, situations are very similar except for the anisotropic deformation of CNT, the carbon networks in ZZ4@$(n,0)$CNT just expand. With the increasing size of $(n,0)$ CNTs for n = 9–11, the expansion ratio reduces from 7.1% to 1.7%, indicating the attenuation of the repulsive interactions. During this process, the corresponding d1 bond has a small change from ∼1.367 Å to ∼1.384 Å, but the d2 bond stretches largely from ∼1.465 Å to ∼1.606 Å. Nevertheless, the lengths of these two bonds are still close to that of a typical N–N single bond (∼1.45 Å). When confined in (12,0) CNT, the repulsive confining potential applied on the polymeric nitrogen are so small that the inward force cannot prevent d2 bond splitting and the square tube is substituted by a rectangular tube as shown in Fig. S7(a). On the other hand, the mechanical stabil-

ity of AC3 seems to be more sensitive to the size of CNT. It will dissolve into three isolated chains when confined in (6,6) CNT as shown in Fig. S2(b). More interestingly, these isolated chains are different from the previously proposed zigzag or armchair chain, it is more likely an enhanced armchair chain possessing three steps instead of two as in the normal armchair chain. The bond lengths in AC3@(5,5)CNT are ∼1.408 Å and ∼1.487 Å for d1 and d2, respectively, they are both larger than that in the ZZ4@(9,9)CNT and closer to the N–N single bond (∼1.45 Å).

To further verify the stability of the combined systems under ambient conditions with finite temperature, AIMD simulations with NVT ensembles were performed, with much larger supercells to meet the commensurability conditions. All the AIMD simulations were performed for 10 ps with the time step of 1 fs under the temperature conditions from 200 K to 400 K. We found that the ZZ1′@$(n,0)$CNT with $n = 8$–12 and ZZ4@$(n,0)$CNT with $n = 9$–10 can remain the chain or tube structure under ambient condition. The structures of these two typical phases at the end of AIMD simulations are presented in Figs. S6 and S7. When confined in a much larger size of (11,0) CNT, the ZZ4 polymeric nitrogen cannot remain in the nanotube structure, it is more likely to dissolve into isolated zigzag chains. The most interesting thing occurred in the system of AC3@(5,5)CNT. At 200 K, it can remain the initial hexagonal nanotube structure with three enhanced armchair chains covalently bonded with each other. However, when heated to 300 K, some parts of the hexagonal tube dissolved, with three armchair chains decoupled. Surprisingly, instead of isolated chains, they turned into bamboo-like nanotube structures. It was attributed to the different and alternative decoupling methods between the two adjacent segments, no isolated armchair chains appeared. The time evolutions of the corresponding bond lengths at the final 2 ps of three typical systems are plotted in Fig. S5.

Discussions—Charge Transfers and Electronic Structures. As reported previously, the stability of the N8 chain can be attributed to the charge transfer between nitrogen and carbon nanotubes.[35,36] Are the stabilization mechanisms of these new phases the same? To answer this question, we calculated the charge density difference between the combined system and the sum of stand-alone nitrogen chain and carbon nanotubes, as displayed in Fig. 3. For ZZ1′@(9,0)CNT, it is evident that electrons are transferred from the carbon nanotube to the nitrogen chain. The Bader charge analysis exhibits that about $0.01e$ are captured by every nitrogen atom in the ZZ1′, which is much smaller than that in N8@CNTs ($0.05e$/atom).[35] In addition, some charge transfers emerge in different directions of the anisotropic CNT. For AC3@(5,5)CNT and ZZ4@(9,0)CNT, however, the most significant phenomenon is that electrons in the vacuum gap between nitrogen and carbon nanotube are transferred to both sides, even though the Bader charge analysis gives the results that each nitrogen atom captures less than $0.01e$ in both phases.

To understand the interaction between nitrogen and carbon nanotubes, we further calculated the electronic structure properties of the combined systems as shown in Fig. 4. The projected band structure and projected density of states (PDOS) of the combined systems are compared with the electronic properties of the stand-alone polymeric nitrogen and carbon nanotubes. From the first glance, the isolated polymeric nitrogen phases are all insulators, the corresponding CNTs are all semiconductors, and the whole combined systems remain semiconducting, this is different from the zigzag N8@(n,0)CNT and armchair N8@(5,5)CNT, which all exhibit metallic properties.[35,36] For ZZ1′@(9,0)CNT, the bands that originated from the CNT are almost the same as in the isolated one, while the valence and conduction bands projected on nitrogen atoms shift downward as compared to the stand-alone ZZ1′. This kind of shift has not much physical meaning because of the uncertainty of Fermi level between the valence band maximum and the conduction band minimum for semiconducting or insulating materials at 0 K. The large charge transfer in the metallic N8@CNTs can be attributed to the band shift near the Fermi level due to the change between the occupied and unoccupied states originating from the strong orbital hybridization. However, the ZZ1′@(9,0)CNT is a semiconductor that no band crosses the Fermi level. When combined, the belongings to the conduction or valence band are well maintained that no significant charge transfer occurs. These phenomena can also be seen in the projected DOS [Figs. 4(b) and 4(c)]. As to the AC3@(5,5)CNT, the magnitude of downward shifts is smaller than that in ZZ1′@(9,0)CNT as shown in Figs. 4(d) and 4(e). The highest two occupied bands coming from nitrogen orbitals have a mixed color indicating stronger orbital overlapping between nitrogen and carbon atoms than that in the ZZ1′@(9,0)CNT. Because each nitrogen atom in the polymeric nanotube has three single bonds and one lone pair electron pointing to the CNT, which provides a strong Coulomb repulsive interaction. When nitrogen atoms are very close to CNT, The electron clouds in the middle will be pushed away to both sides as shown in Fig. 3. On the contrary, when encapsulated into a much larger size of CNT, the orbital overlapping is so small that polymeric nitrogen feels a very weak repulsive potential. They cannot be stabilized by charge transfer only and will

be decomposed into isolated chains. Therefore, the proper size of CNTs is necessary to provide a strong repulsive force for the stability of these novel nanotube structures. In the electronic structure calculations, all of the results are based on the commensurate systems, there should be lattice mismatch and longitudinal stress between CNT and nitrogen species. In the ideal incommensurate systems, the overall longitudinal stress may disappear, however, the confinement in the radial direction should be quite similar to our commensurate structures. In addition, as we can see, no bonds are formed between nitrogen and carbon atoms, the charge transfers are also small, the mutual interaction should be dominated by the whole systems instead of the local environments. The commensurate structures used in our calculations should have a small influence on the electronic properties compared to the ideal incommensurate structures.

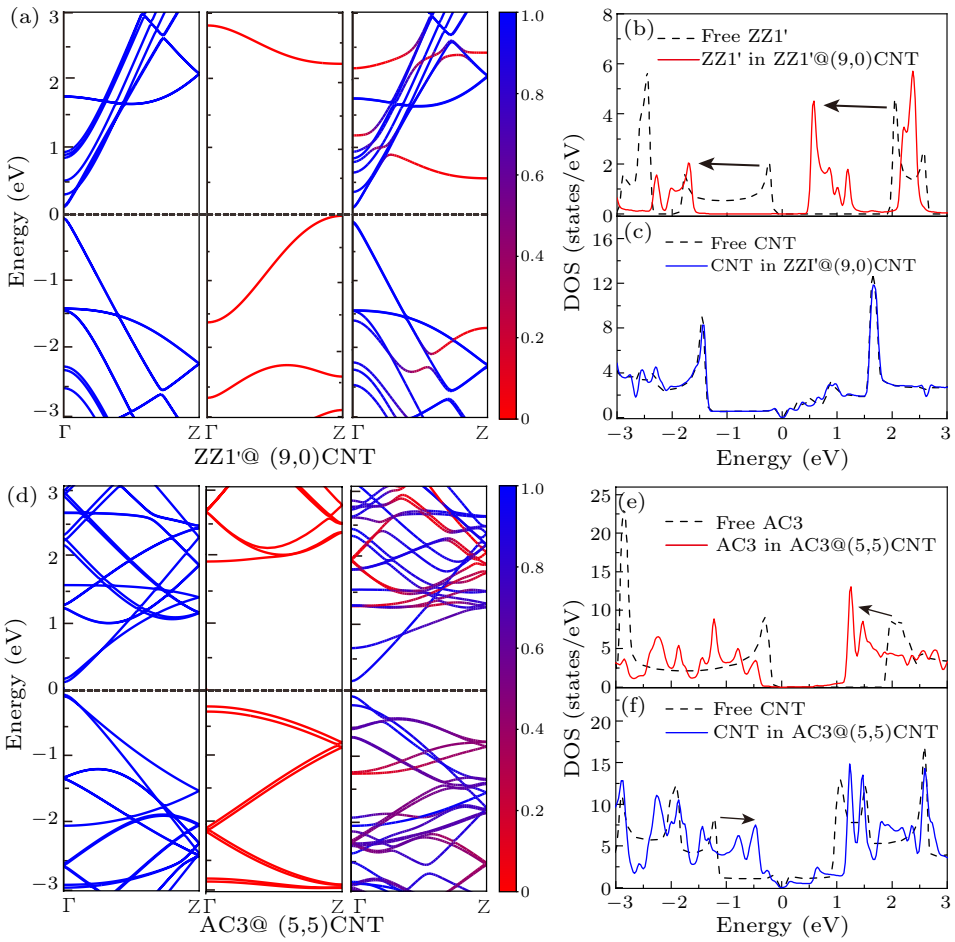

Fig. 4. The projected band structures and density of states of the combined systems of ZZ1′@(9,0)CNT and AC3@(5,5)CNT. The corresponding electronic properties of the isolated nitrogen and carbon nanotube are also shown for comparison. Contributions originated from carbon nanotubes and nitrogen are plotted with blue and red colors respectively. The black arrows indicate the shift of the DOS peaks when they are combined.

The cubic gauge nitrogen allotrope has been synthesized within the short-length multi-wall carbon nanotubes at near-ambient pressure using plasma-enhanced chemical vapor deposition,[36] which provides some inspiration for possible synthesis of the obtained combined systems proposed in this work. Short-length CNTs are needed to allow for the samples to go inside the tubes and the sodium azides can be used as a good precursor for synthesizing polymeric nitrogen, the alkali metal sodium can provide extra electrons to reduce the reaction energy barrier. The short-length CNTs powder together with the sodium azide can be loaded into the DAC. The mixture of argon and nitrogen can be used as the pressure transfer medium. When the samples are laser heated to specified temperatures, the polymeric nitrogen may form within the CNTs.

High Energy Density. Since the polymeric nitrogen nanotube will release a large amount of energy when decomposed into isolated nitrogen molecules and then squeezed out from the carbon nanotube, these combined nanotube phases may be considered to be

a new type of high energy density materials. Figure 5 and Table S4 show the calculated energy densities of these combined systems. The polymeric nitrogen-filled CNT bundles with a hexagonal lattice were employed for the energy density calculations instead of a single isolated nitrogen-filled CNT. To make a comparison, the results from the typical explosive TNT are also listed.[42,43]

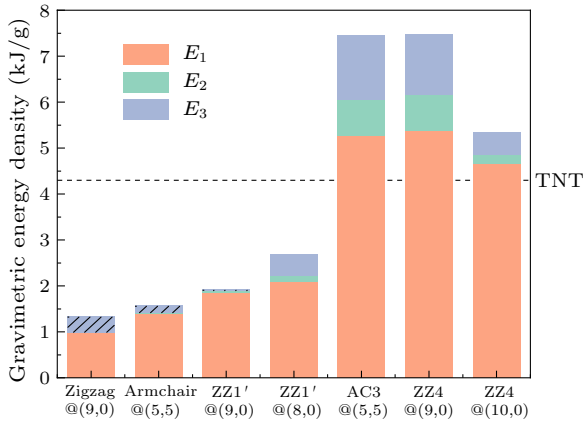

Fig. 5. The calculated gravimetric energy density of several combined systems. The total energy densities are composed of three parts, the decomposition energy (E_1) from polymeric nitrogen to isolated molecules, the deformation energy (E_2) of CNT, and the combining energy (E_3) between the polymeric nitrogen and carbon nanotube. The dashed reference line at 4.3 represents the result of TNT, the shadow areas indicate that the combining energies are negative.

Our calculated results show that the energy density of single nitrogen chain systems, such as zigzag@(9,0)CNT, armchair@(5,5)CNT, and ZZ1′@(9,0)CNT are rather lower than that of TNT (4.3 kJ/g).[43] However, for these systems with nanotube structures, the gravimetric energy densities of AC3@(5,5)CNT (7.46 kJ/g) and ZZ4@(9,0)CNT (7.49 kJ/g) are almost twice of TNT. The corresponding volumetric energy densities are 17.68 kJ/cm^3 and 17.78 kJ/cm^3, respectively, which are even higher than twice of TNT(7.05 kJ/cm^3). It is worth noting that the obtained energy density for ZZ4@(10,0)CNT (5.34 kJ/g) has an obvious reduction as compared to ZZ4@(9,0)CNT (7.49 kJ/g). The total energy density can be classified into three different parts (illustrated in Fig. S12), i.e., the decomposition energy from polymeric nitrogen to isolated nitrogen molecules, the deformation energy of CNT, and the combining energy between polymeric nitrogen and CNT. It is clear that the combining energies for most of the chain polymer systems are negative but the results for these nanotube polymers are positive. Because the (8,0) CNT has a small radius, the interactions between nitrogen and CNT is repulsive and the combining energy is positive. The corresponding three parts for ZZ4@(9,0)CNT are 5.382 kJ/g, 0.781 kJ/g, and 1.322 kJ/g, respectively, the most significant part comes from the decomposition of polymeric nitrogen. Therefore, the polymeric nitrogen nanotube systems possess a very high energy density, which is almost twice that of the typical explosive materials TNT. Most of the energy density comes from the decomposition of polymeric nitrogen, while the deformation energy of CNT and the combining energy between the two parts are also not negligible.

In summary, we have developed a new scheme of crystal structure searching in a confined space combining the conventional crystal structure search method with external confining potentials fitted from first-principles calculations. With this approach, we systematically searched the polymeric nitrogen inside carbon nanotubes and identified three new polymeric nitrogen phases stabilized in carbon nanotubes. Instead of chain polymer, two of them are composed of nitrogen tubes. The experimental synthesis of cg-N with the help of CNT under the ambient condition indicates that these phases may also be synthesized experimentally. These two nanotube phases are both single-bonded therefore possess a high energy density that is almost twice the value of TNT. These newly predicted combined materials are all semiconductors or insulators. For ZZ1′@(9,0)CNT, anisotropic deformation of CNT and charge transfer all help stabilize the structure. However, for AC3@(5,5)CNT and ZZ4@(9,0)CNT, charge transfers are very different in that electrons in the middle space are squeezed out to both sides. The strong repulsive confining potential arising from Coulomb interaction is the main factor for the stabilization of the combined system. Due to this reason, only carbon nanotubes with special sizes are capable of stabilizing polymeric nitrogen nanotubes. Here we only focus on the stability of the polymeric nitrogen with the help of the confining potentials of carbon nanotubes, syntheses of these polymeric nitrogen structures remain a challenge due to the requirement of the opening of the very strong N≡N triple bond. However, our work still provides a new strategy for exploring novel high energy density polymeric nitrogen materials, as well as the synthesis of other nanomaterials with the help of the confining space inside framework structures, such as nanotubes, zeolites, and covalently bonded frameworks.

Methods. Geometry optimizations and electronic structure analysis were performed in the framework of density functional theory within generalized gradient approximation (GGA) using Perdew–Burke–Ernzerhof (PBE) functionals[44] as implemented in the VASP package.[45] A projector augmented wave (PAW)[46] potentials with the plane-wave kinetic energy cutoff 600 eV were adopted. The Monkhorst-pack[47] methods were applied with $1 \times 1 \times k_z$ meshes.

Here the k_z sampling is less than $2\pi \times 0.03\,\text{Å}^{-1}$ along the c axis. We optimize the structures with the convergence criteria of less than $1 \times 10^{-4}\,\text{eV/Å}$ and $1 \times 10^{-5}\,\text{eV}$ for internal force and total energy per atom, respectively. All the phonon frequencies were calculated using a finite displacements method as implemented in the PHONOPY[48] package together with the VASP code. The structures are only expanded in the direction of c with $1 \times 1 \times 3$ supercells. The forces within the supercells with some displacements were calculated with the ICNTs and the convergence criteria for the energy is less than $1 \times 10^{-5}\,\text{eV}$ per atom (see the Supplemental Information for more details).

Acknowledgments. J.S. thanks the financial support from the National Natural Science Foundation of China (Grant Nos. 12125404, 11974162, and 11834006), and the Fundamental Research Funds for the Central Universities. The calculations were carried out using supercomputers at the High Performance Computing Center of Collaborative Innovation Center of Advanced Microstructures, the high-performance supercomputing center of Nanjing University.

References

[1] Mailhiot C, Yang L H, and McMahan A K 1992 *Phys. Rev. B* **46** 14419
[2] Eremets M I, Gavriliuk A G, Trojan I A, Dzivenko D A, and Boehler R 2004 *Nat. Mater.* **3** 558
[3] Ma Y, Oganov A R, Li Z, Xie Y, and Kotakoski J 2009 *Phys. Rev. Lett.* **102** 065501
[4] Pickard C J and Needs R J 2009 *Phys. Rev. Lett.* **102** 125702
[5] Wang X, Wang Y, Miao M, Zhong X, Lv J, Cui T, Li J, Chen L, Pickard C J, and Ma Y 2012 *Phys. Rev. Lett.* **109** 175502
[6] Sun J, Martinez-Canales M, Klug D D, Pickard C J, and Needs R J 2013 *Phys. Rev. Lett.* **111** 175502
[7] Tomasino D, Kim M, Smith J, and Yoo C S 2014 *Phys. Rev. Lett.* **113** 205502
[8] Ji C, Adeleke A A, Yang L X, Wan B, Gou H Y, Yao Y S, Li B, Meng Y, Smith J S, Prakapenka V B, Liu W J, Shen G Y, Mao W L, and Mao H K 2020 *Sci. Adv.* **6** eaba9206
[9] Laniel D, Winkler B, Fedotenko T, Pakhomova A, Chariton S, Milman V, Prakapenka V, Dubrovinsky L, and Dubrovinskaia N 2020 *Phys. Rev. Lett.* **124** 216001
[10] Eremets M I, Popov M Y, Trojan I A, Denisov V N, Boehler R, and Hemley R J 2004 *J. Chem. Phys.* **120** 10618
[11] Christe K O 2007 *Propell.Explos. Pyrotech.* **32** 194
[12] Laniel D, Geneste G, Weck G, Mezouar M, and Loubeyre P 2019 *Phys. Rev. Lett.* **122** 066001
[13] Lei L, Tang Q Q, Zhang F, Liu S, Wu B B, and Zhou C Y 2020 *Chin. Phys. Lett.* **37** 068101
[14] Peng F, Yao Y, Liu H, and Ma Y 2015 *J. Phys. Chem. Lett.* **6** 2363
[15] Xu Y, Wang Q, Shen C, Lin Q, Wang P, and Lu M 2017 *Nature* **549** 78
[16] Zhang C, Sun C G, Hu B C, Yu C M, and Lu M 2017 *Science* **355** 374
[17] Huang B and Frapper G 2018 *Chem. Mater.* **30** 7623
[18] Xia K, Yuan J, Zheng X, Liu C, Gao H, Wu Q, and Sun J 2019 *J. Phys. Chem. Lett.* **10** 6166
[19] Bykov M, Chariton S, Bykova E, Khandarkhaeva S, Fedotenko T, Ponomareva A V, Tidholm J, Tasnadi F, Abrikosov I A, Sedmak P, Prakapenka V, Hanfland M, Liermann H P, Mahmood M, Goncharov A F, Dubrovinskaia N, and Dubrovinsky L 2020 *Angew. Chem. Int. Ed. Engl.* **59** 10321
[20] Yuan J, Xia K, Wu J, and Sun J 2021 *Sci. Chin. Phys. Mech. & Astron.* **64** 218211
[21] Niu S, Li Z, Li H, Shi X, Yao Z, and Liu B 2021 *Inorg. Chem.* **60** 6772
[22] Salke N P, Xia K, Fu S, Zhang Y, Greenberg E, Prakapenka V B, Liu J, Sun J, and Lin J F 2021 *Phys. Rev. Lett.* **126** 065702
[23] Steele B A and Oleynik I I 2016 *Chem. Phys. Lett.* **643** 21
[24] Laniel D, Winkler B, Koemets E, Fedotenko T, Bykov M, Bykova E, Dubrovinsky L, and Dubrovinskaia N 2019 *Nat. Commun.* **10** 4515
[25] Bykov M, Fedotenko T, Chariton S, Laniel D, Glazyrin K, Hanfland M, Smith J S, Prakapenka V B, Mahmood M F, Goncharov A F, Ponomareva A V, Tasnádi F, Abrikosov A I, Bin M T, Hotz I, Rudenko A N, Katsnelson M I, Dubrovinskaia N, Dubrovinsky L, and Abrikosov I A 2021 *Phys. Rev. Lett.* **126** 175501
[26] Zhang J, Niu C, Zhang H, Zhao J, Wang X, and Zeng Z 2021 *J. Phys. Chem. Lett.* **12** 5731
[27] Medeiros P V C, Marks S, Wynn J M, Vasylenko A, Ramasse Q M, Quigley D, Sloan J, and Morris A J 2017 *ACS Nano* **11** 6178
[28] Slade C A, Sanchez A M, and Sloan J 2019 *Nano Lett.* **19** 2979
[29] Wang Z X, Ke X Z, Zhu Z Y, Zhang F S, Ruan M L, and Yang J Q 2000 *Phys. Rev. B* **61** R2472
[30] Sandoval S, Tobias G, and Flahaut E 2019 *Inorg. Chim. Acta* **492** 66
[31] Gimondi I and Salvalaglio M 2018 *Mol. Syst. Des. Eng.* **3** 243
[32] Lei S, Paulus B, Li S, and Schmidt B 2016 *J. Comput. Chem.* **37** 1313
[33] Fujimori T, Morelos-Gomez A, Zhu Z, Muramatsu H, Futamura R, Urita K, Terrones M, Hayashi T, Endo M, Hong S Y, Choi Y C, Tomanek D, and Kaneko K 2013 *Nat. Commun.* **4** 2162
[34] Thang P, Oh S, Stonemeyer S, Shevitski B, Cain J D, Song C, Ercius P, Cohen M L, and Zettl A 2020 *Phys. Rev. Lett.* **124** 206403
[35] Abou-Rachid H, Hu A, Timoshevskii V, Song Y, and Lussier L S 2008 *Phys. Rev. Lett.* **100** 196401
[36] Li Y, Bai H, Lin F, and Huang Y 2018 *Physica E* **103** 444
[37] Benchafia E M, Yao Z, Yuan G, Chou T, Piao H, Wang X, and Iqbal Z 2017 *Nat. Commun.* **8** 930
[38] Ji W, Timoshevskii V, Guo H, Abou-Rachid H, and Lussier L S 2009 *Appl. Phys. Lett.* **95** 021904
[39] Liu S J, Yao M G, Ma F X, Liu B, Yao Z, Liu R, Cui T, and Liu B B 2016 *J. Phys. Chem. C* **120** 16412
[40] Liu S, Li H Y, Yao Z, and Lu S C 2021 *Mater. Today Commun.* **26** 101670
[41] Xia K, Gao H, Liu C, Yuan J N, Sun J, Wang H T, and Xing D Y 2018 *Sci. Bull.* **63** 817
[42] Kamlet M J and Dickinson C 1968 *J. Chem. Phys.* **48** 43
[43] Zhang J, Oganov A R, Li X, and Niu H 2017 *Phys. Rev. B* **95** 020103
[44] Perdew J P, Burke K, and Ernzerhof M 1996 *Phys. Rev. Lett.* **77** 3865
[45] Kresse G and Furthmuller J 1996 *Phys. Rev. B* **54** 11169
[46] Blöchl P E 1994 *Phys. Rev. B* **50** 17953
[47] Monkhorst H J and Pack J D 1976 *Phys. Rev. B* **13** 5188
[48] Togo A, Oba F, and Tanaka I 2008 *Phys. Rev. B* **78** 134106

Supplemental Information for

"High energy density polymeric nitrogen inside carbon nanotubes"

Chi Ding(丁驰)[1], Junjie Wang(王俊杰)[1], Yu Han(韩瑜)[1], Jianan Yuan(袁嘉男)[1],

Hao Gao(高豪)[1], and Jian Sun(孙建)[1,*]

[1]*National Laboratory of Solid State Microstructures,*

School of Physics and Collaborative Innovation Center of Advanced Microstructures,

Nanjing University, Nanjing, 210093, China

Contents

I. Structure search and implicit confining potentials;

II. Additional polymeric structures identified in our work;

III. Enthalpy results;

IV. Phonon spectrum and AIMD simulation results;

V. The size effects of carbon nanotubes on the structure of polymeric nitrogen;

VI. The temperature effects on the combined systems;

VII. Electronic properties;

VIII. Illustration of the energy density calculation;

IX. Coordinates for several of the typical structures.

* Corresponding author. jiansun@nju.edu.cn

I. Structure search and implicit confining potentials

In this article, we developed a new scheme of crystal structure searching in a confined space and employed it to predict polymeric nitrogen structures inside carbon nanotubes. The initial cells were set to be tetragonal with the cell parameters in *a*, *b* directions being 15 Å, and the length of the *c* axis being generated randomly. Because the confining potentials were in the *a*, *b* plane, the initial one-dimensional nitrogen structures were set to be in the *c* axis and it is periodic along this direction, the vacuum space in the *a*, *b* directions are larger than 10 Å between adjacent nitrogen polymers. There are 8, 10, 12, 16, 20, 24 nitrogen atoms in the cell respectively for every search. The external pressure was applied only along the *c* direction and the vertical pressure is defined as the uniaxial stress: $P = \sigma_{zz}$. The uniaxial stress is not conserved with varying bottom surface area[1]. The conserved quantities are the forces acting on the bottom surface: $F_z = \sigma_{zz}^{'} \cdot S^{'}$, where $S^{'}$ is the bottom surface area and $\sigma_{zz}^{'}$ is the calculated uniaxial stress[1]. In practical CNT bundles, the CNTs take the close-packed hexagonal configuration with the bottom surface area *S*. Because the polymeric nitrogen is finally loaded into the CNT bundles, the uniaxial stress for the quasi-1D polymeric nitrogen can be defined as $\sigma_{zz} = F_z/S$. In the structure optimization, we fixed the cell parameters in the *a*, *b* directions and only optimize the *c* axis until the vertical stress tensor converged to a target pressure. To make a thorough search for polymeric nitrogen phases inside CNTs, systematic crystal structure searches were performed for cells containing up to 24 nitrogen atoms with vertical pressures of 0, 2, 5, and 10 GPa.

To reduce the computational cost during the structure searching, external cylindrical confining potentials were introduced to represent the corresponding carbon nanotubes. We first calculated the binding energy of CNT and a nitrogen molecule versus their distance. Two different nitrogen configurations with the nitrogen molecule perpendicular and parallel to the *c* axis of the carbon nanotube were taken into consideration, they give very similar results. We also took into considerations of several van der walls interactions such as DFT-D3[2] and PBE+optB86b[3], they have little influence on the small size of CNTs. If not specified, we take the results from the parallel configuration with the optB86b functional in the following enthalpy calculations. These calculated results were well fitted to a Lennard-Jones type analytical potential $V(\mathrm{r}) = D \cdot \left(\left(\frac{k}{r+a}\right)^{12} - \left(\frac{k}{r+a}\right)^{6} +\right.$

$\left(\frac{k}{r-a}\right)^{12} - \left(\frac{k}{r-a}\right)^{6}\right)$, where r represent the distance between the center of nitrogen molecule and the center of CNTs. The calculated and fitted energy profiles for the (10, 0) CNT were plotted in Fig. S1(c), and the corresponding parameters of D, k and a for different carbon nanotubes were shown in Table. S1.

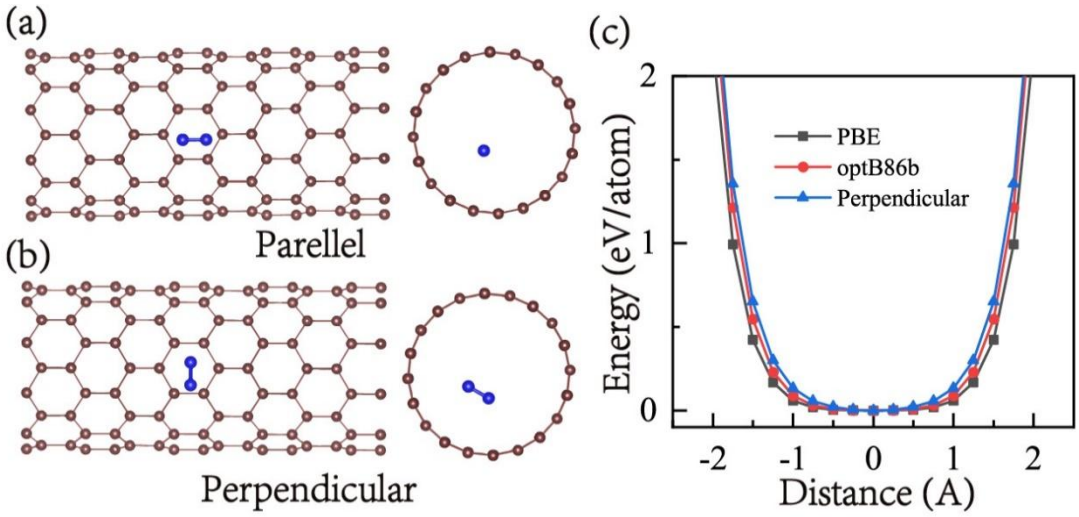

Figure S1. The Parallel (a) and Perpendicular (b) orientation of nitrogen unit in a typical (10, 0) carbon nanotube. (c) Calculated confining potentials of the parallel configuration with the PBE and optB86b functional, and of the perpendicular configuration.

Table S1. The diameters *d* of corresponding CNTs and the calculated parameters of *D*, *k* and *a* fitted to the energy profiles between nitrogen and CNTs.

	(5, 5)	(6, 6)	(7, 7)	(8, 0)	(9, 0)	(10, 0)	(11, 0)	(12, 0)
d /Å	6.78	8.14	9.49	6.26	7.05	7.83	8.61	9.39
D	24.3	1.49	0.8	23.0	8.45	7.56	1.10	0.85
k	8.68	6.13	5.66	8.33	7.30	7.62	5.92	5.77
a	10.6	7.70	7.77	9.96	8.92	9.59	7.67	7.83

II. Additional polymeric structures identified in our work;

There are several other types of polymeric nitrogen phases identified in our research work. Except for the one single polymeric nitrogen structure, several chains can be encapsulated together in one single cylindrical carbon nanotube. For example, two of the proposed ZZ1' phase can be loaded into the (n, 0) CNT as presented in Fig. S2 (a). These two chains are parallel to each other with the extra nitrogen atom in the opposite side of the zigzag chains. Three enhanced armchair chains can be confined in the (6, 6) CNT with a triangular configuration as shown in Fig. S2 (b). There are three steps in the enhanced armchair chain as denoted with the number, which is different from the normal armchair chain with two steps. This system is also what we obtained in the AIMD simulations when the AC3 were encapsulated into the much larger size of (6, 6) CNT. In addition, Fig. S2 (c) displayed a square nitrogen nanotube achieved in the (11, 0) CNT. The nitrogen polymer were composed of four zigzag chains the same as in the ZZ4 structure, but these chains are linked by one extra nitrogen atom instead of covalently bonded with each other directly. More interestingly, the four extra atoms linking every two zigzag chains as denoted with 1-4 are not in the same plane perpendicular to *c* axis, instead they form a helical structural along c axis. These three polymeric nitrogen structures were named as ZZ4', 2ZZ1' and 3eAC.

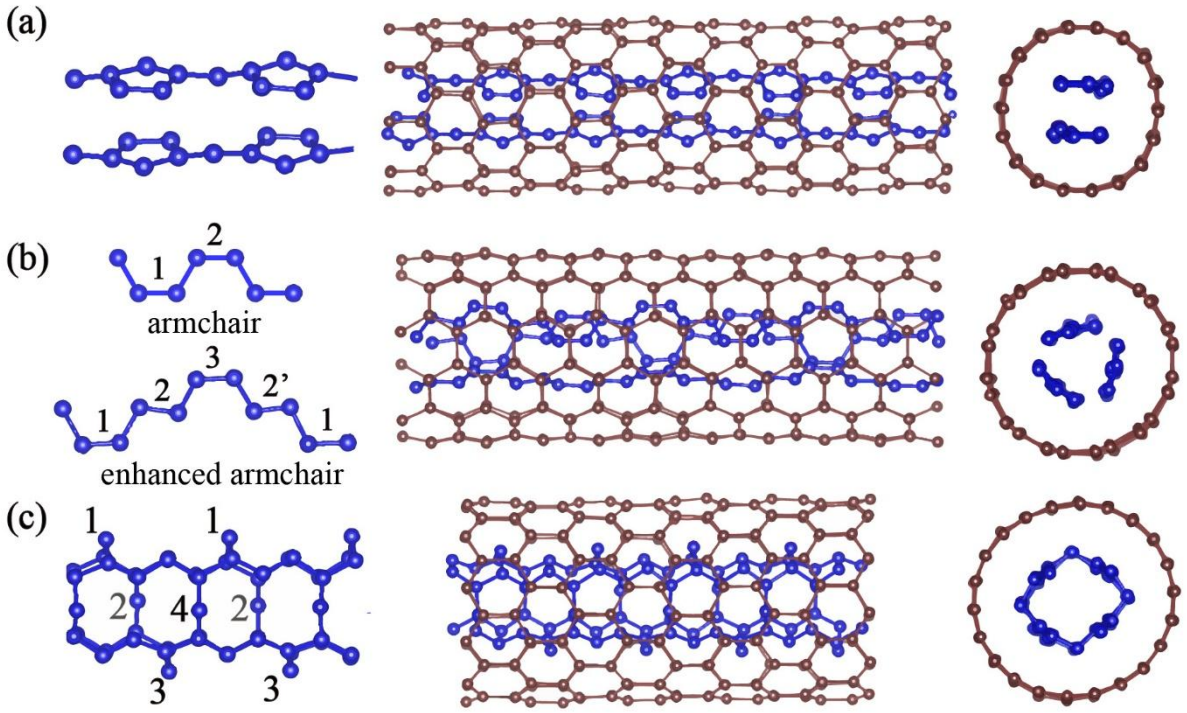

Figure S2. The Top and side view of three structures 2ZZ1', 3eAC and ZZ4' confined in (10, 0), (11, 0) and (6, 6) carbon nanotubes after AIMD simulations at 300K.

III. Enthalpy results

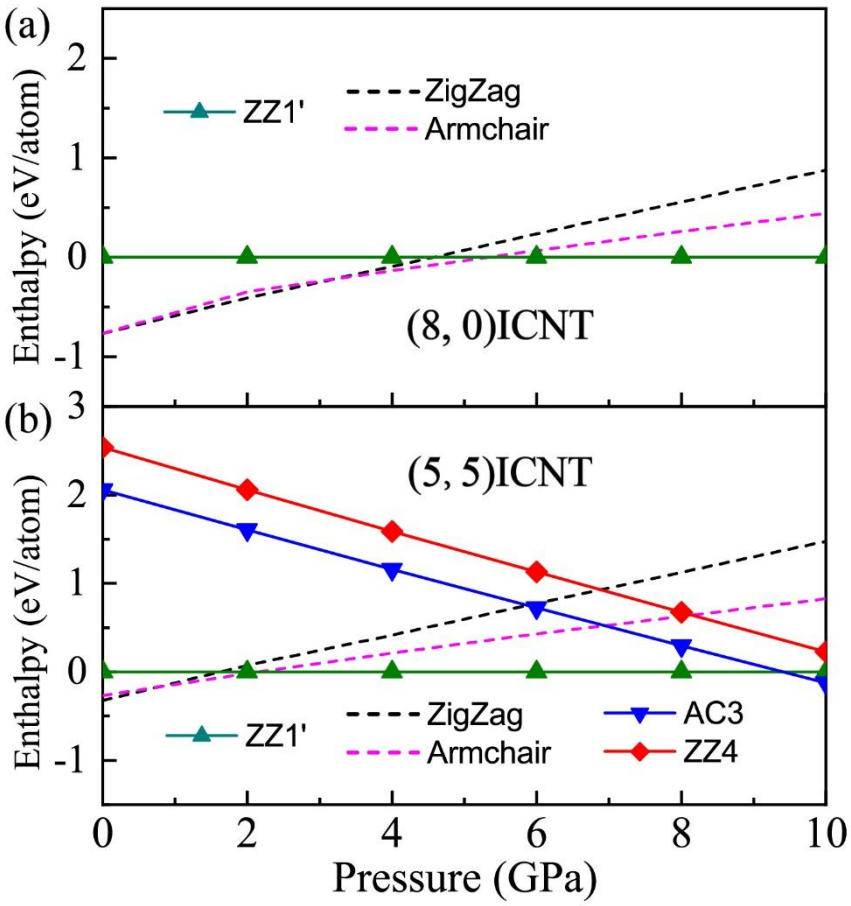

Figure S3. The enthalpy results of polymeric nitrogen structures confined within (a) (8, 0) ICNT and (b) (5, 5) ICNT. Because the (8, 0) CNT has a very small diameter of 6.26 Å, it can only accommodate the chain like polymeric structures, thus only the results for ZZ1', Zigzag and Armchair phases are presented

IV. Phonon spectra and AIMD simulation results

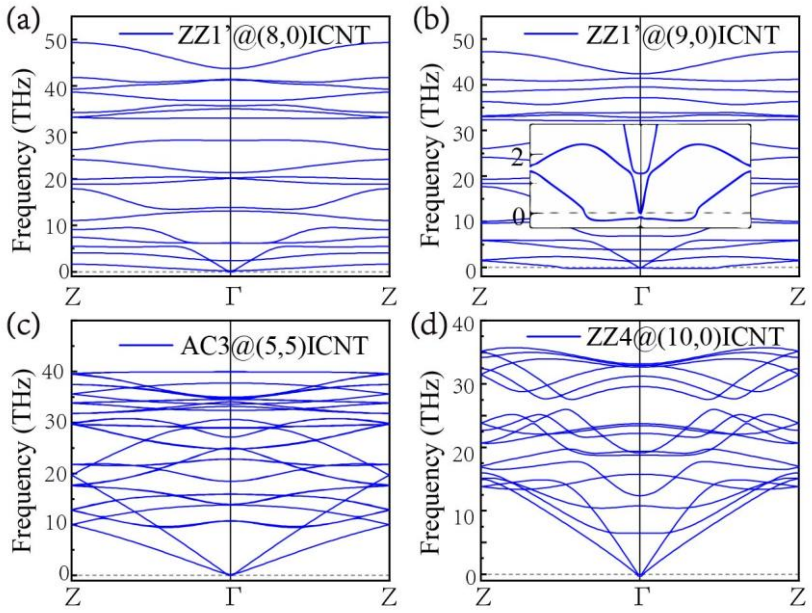

Figure S4. Phonon dispersive curves for ZZ1'@(8,0)ICNT, ZZ1'@(9,0)ICNT, AC3@(5,5)ICNT and ZZ4@(10,0)CNT at ambient vertical pressure.

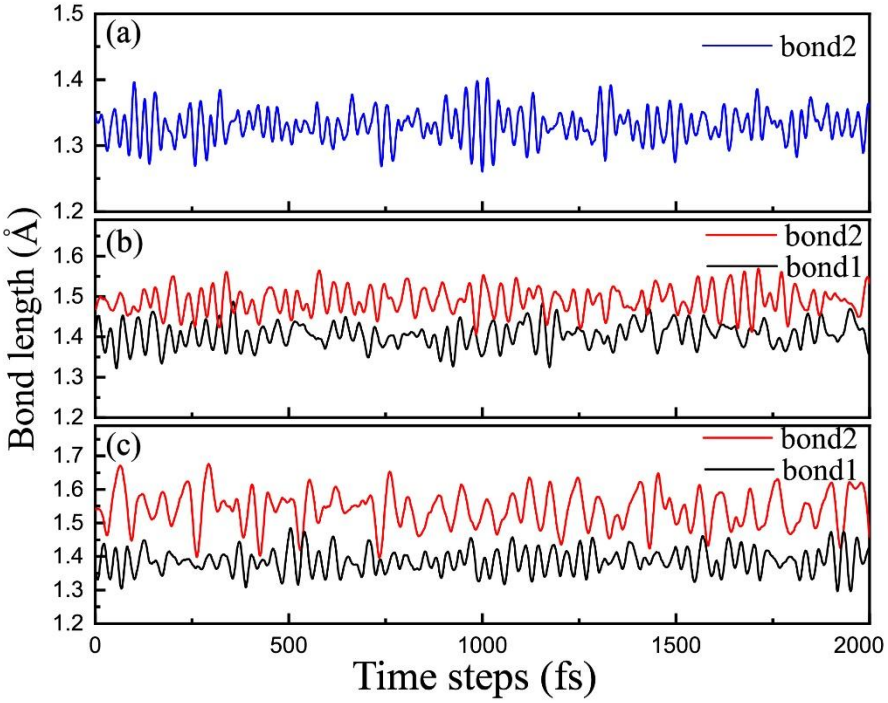

Figure S5. The evolution of bond length in the final 2000fs of three typical phases (a) ZZ1'@(9,0)CNT at 300K, (b)AC3@(5,5)CNT at 200K and (c) ZZ4@(10,0)CNT) at 300K.

V. The size effect of carbon nanotubes on the structure of polymeric nitrogen

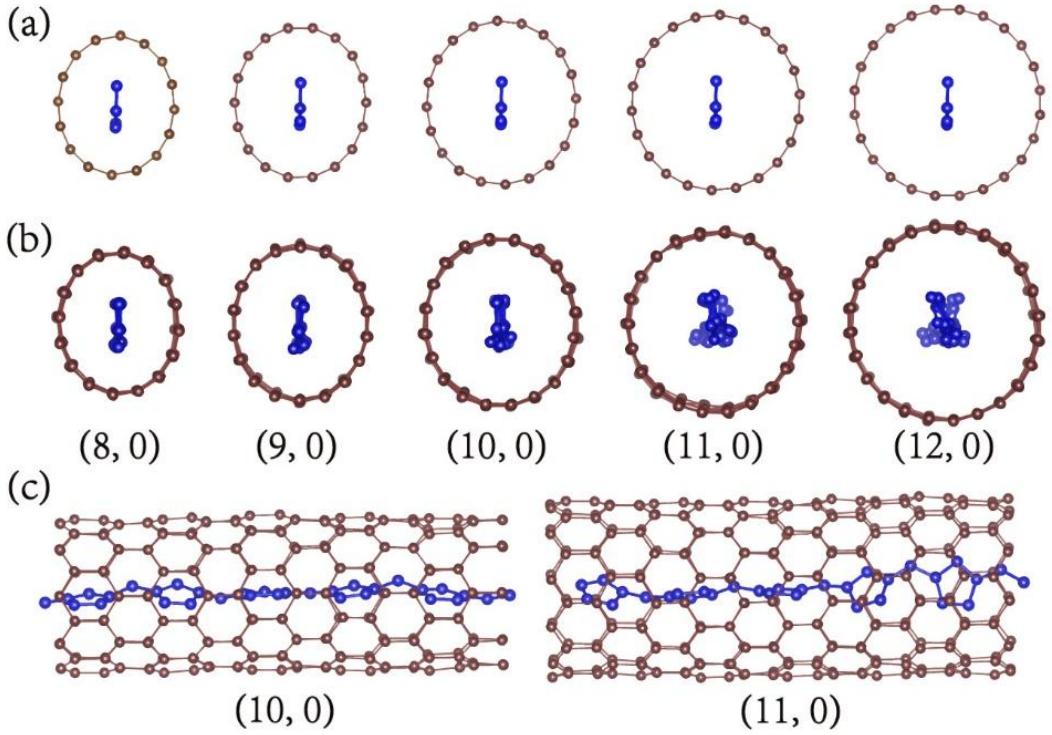

Figure S6. Polymeric ZZ1' nitrogen confined in different size of carbon nanotubes. The top view of these structures after geometry optimization (a) and after MD simulation (b) at 300K. (c) The side view of two typical systems with few and much twist after MD simulation.

Table S2. Four different bond length (d1, d2, d3 and d4) of polymeric ZZ1' phase confined in (n, 0) CNT with n=8-12. The semi-major (a) and semi-minor (b) axis of the fully optimized elliptical carbon nanotubes, their deformation ratio (δ_{ab}) and the radius of the origin circular CNTs (R0).

	a	b	δ_{ab}	R0	d1	d2	d3	d4	average
(8, 0)	3.509	2.927	19.9%	3.166	1.316	1.322	1.318	1.324	1.320
(9, 0)	3.757	3.316	13.3%	3.527	1.327	1.329	1.338	1.331	1.331
(10, 0)	4.122	3.766	9.4%	3.985	1.331	1.331	1.348	1.331	1.335
(11, 0)	4.421	4.233	4.4%	4.379	1.332	1.333	1.351	1.331	1.337
(12, 0)	4.685	4.674	0.2%	4.685	1.333	1.333	1.353	1.331	1.338

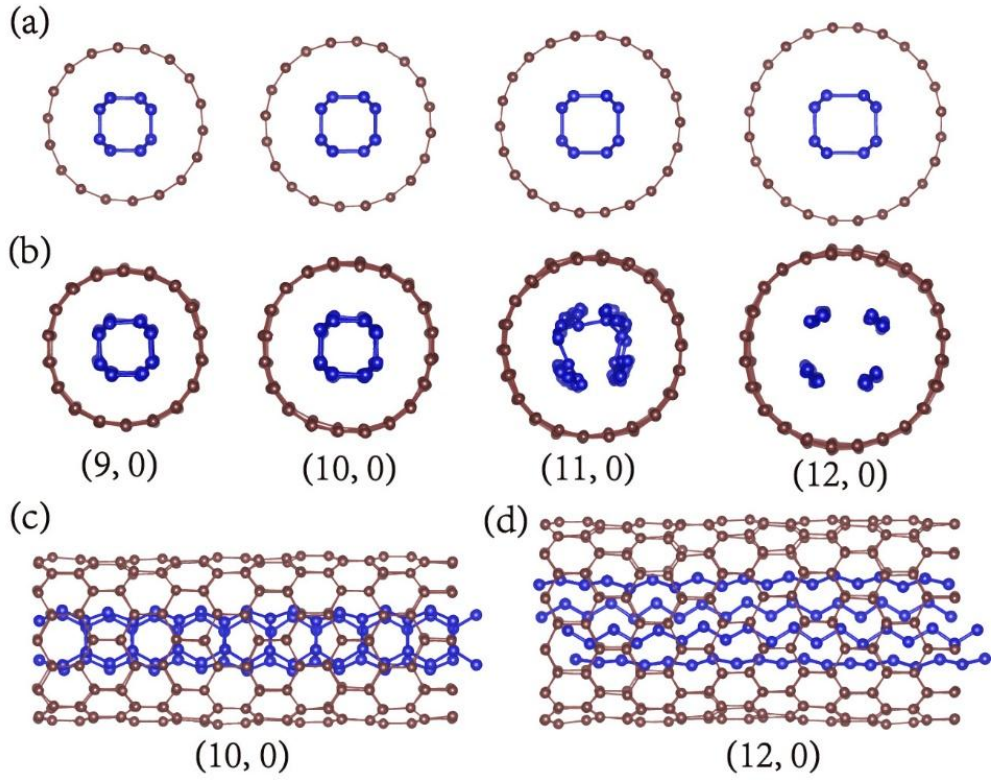

Figure S7. Polymeric ZZ4 nitrogen nanotube confined in different size of carbon nanotubes. The top view of these structures after geometry optimization (a) and after MD simulation at 300K (b). The side view of two typical systems confined in (10, 0) CNT (c) and (12, 0) CNT (d) after MD simulations.

Table S3. Calculated lattice parameter of ZZ4@(n,0)CNT (n=9-11). Including the radius of CNT before and after encapsulated with nitrogen (R0 and R), their deformation ratio (δ_R) and the bond-length of N-N (d1 and d2).

	R0	R	δ_R	d1	d2
(9, 0)	3.538	3.789	7.1%	1.367	1.465
(10, 0)	3.920	4.096	4.5%	1.379	1.525
(11, 0)	4.312	4.384	1.7%	1.384	1.606

VI. The temperature effects on the combined systems

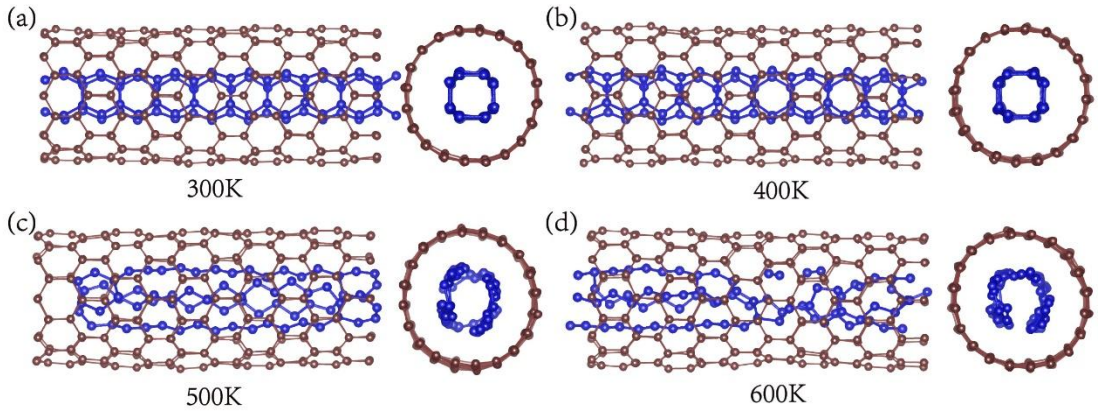

Figure S8. Polymeric ZZ4 nitrogen nanotube confined in (10,0)CNT at different temperatures from 300K to 600K.

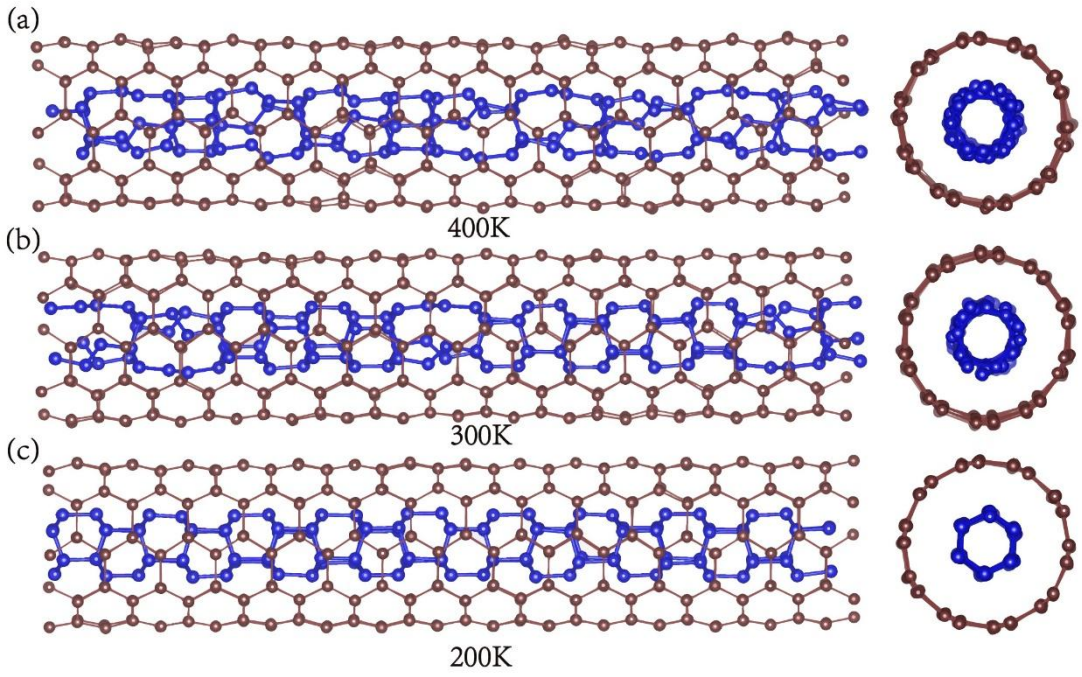

Figure S9. Structures of AC3 confined in (5,5) CNT after MD simulations at temperatures from 200K to 400K. The optimized radius of isolated (5, 5) CNT at 0K is about 3.4 Å, which expands to 3.65 Å after the filling of polymeric nitrogen AC3, the corresponding deformation ratio of CNT is about 7.35%.

VII. Electronic properties

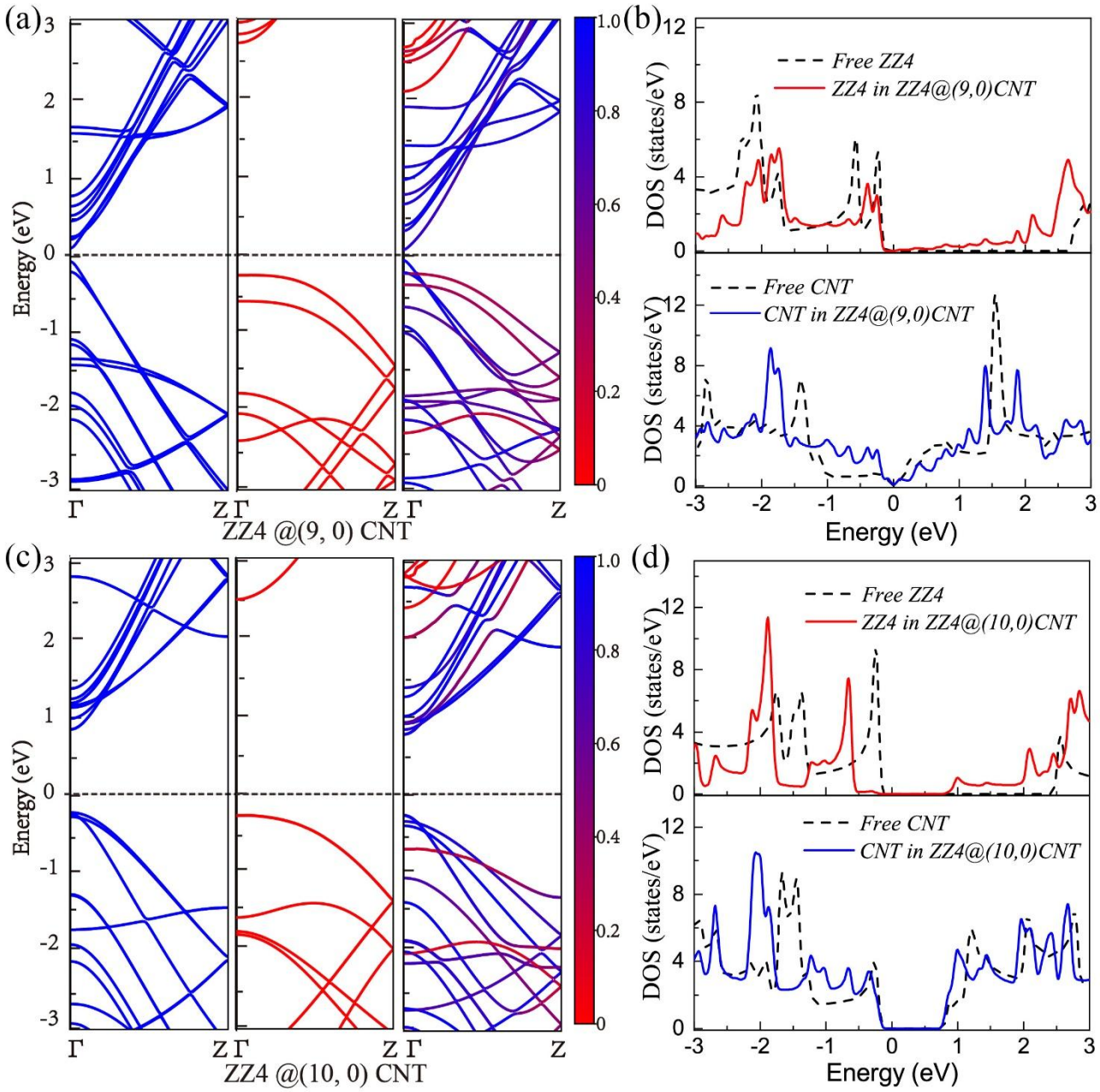

Figure S10. The electronic properties of ZZ4 confined in (9,0) and (10,0)CNT respectively.

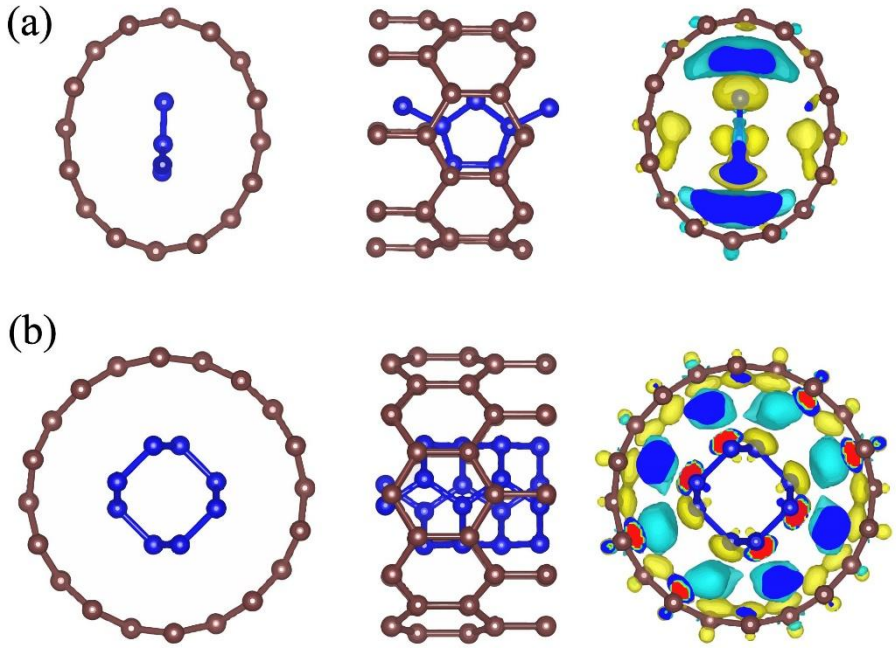

Figure S11. Top and side view of the optimized structures of two combined systems: (a) ZZ1'@(8,0)CNT and (b) ZZ4@(10,0)CNT, and the charge density difference between the combined systems and the sum of stand-alone nitrogen and carbon nanotube with the isosurface values $0.8\text{x}10^{-3}$ and $0.9\text{x}10^{-3}$ respectively.

VIII. Illustration of the energy density calculation

We calculated the gravimetric energy density of these combined systems with the following formula:

$$E_d = [E_{combined} - E_{CNT} - (E_{\alpha-N} - 0.25) * N]/M$$

and then the volumeric energy density is calculated with $E_v = E_d * M/V$. In the formula above, $E_{combined}$ and E_{CNT} represents the energy of the combined systems and the fully optimized carbon nanotube after removing polymeric nitrogen, respectively. *N* is the number of nitrogen atoms, *M* represents the mass of the combined systems, *V* are taken as the volume of corresponding carbon nanotube bundles with a hexgonal lattice. The number "0.25" in above formula represents the reduction of the free energy from the molecular crystal α-N to nitrogen gas[4].

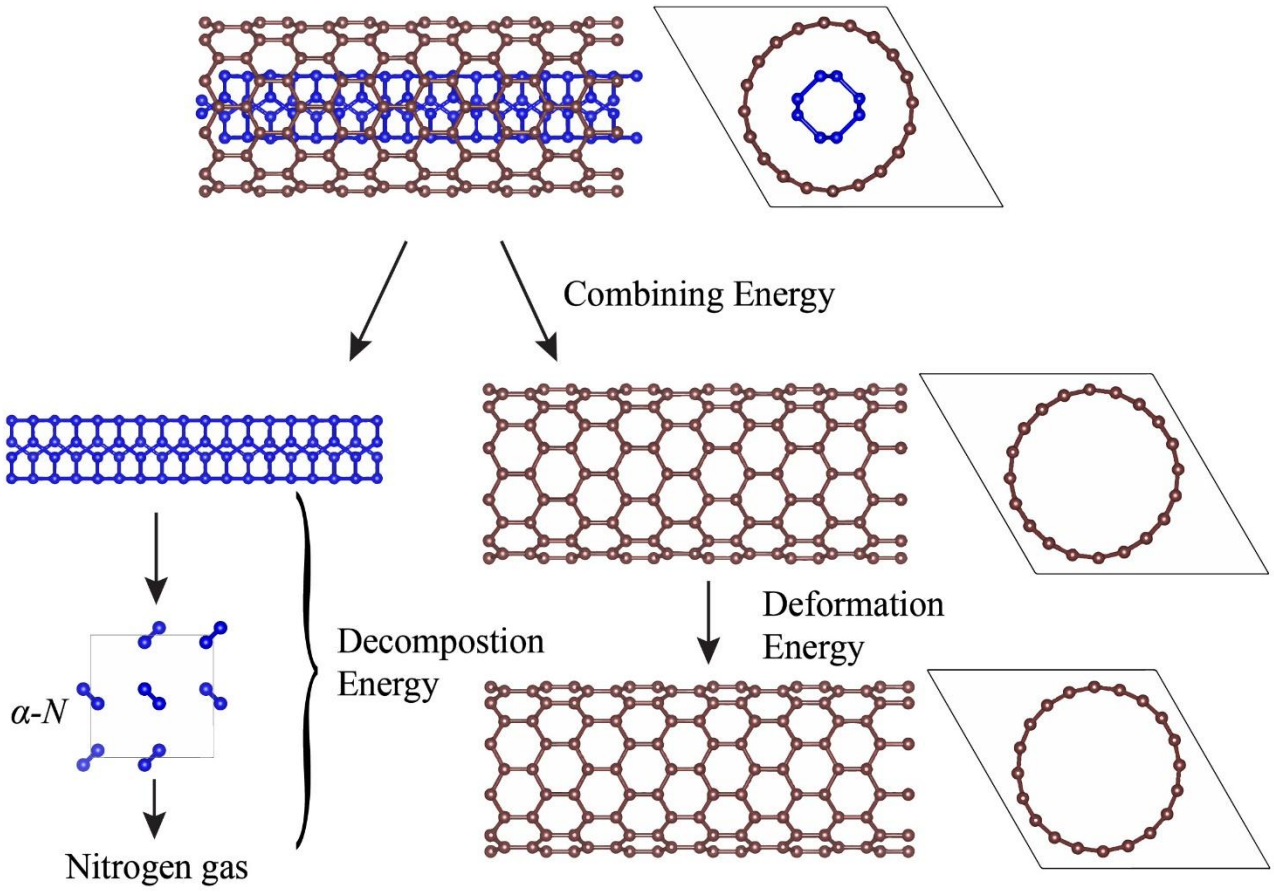

Figure S12. Illustration of the total and parts of the energy density calculations.

Table. S4. The density (ρ), gravimetric (E_d) and volumetric (E_v) energy density of these combined systems compared to the experiment results of the known TNT explosive. The total energy densities are composed by three parts, the decomposition energy (E_1) from polymeric nitrogen to isolated molecules, the deformation energy (E_2) of CNT and the combining energy (E_3) between the polymeric nitrogen and carbon nanotube.

Systems	ρ (g/cm^{-3})	$E_d(kJ/g)$	$E_v(kJ/cm^{-3})$	E_1 (kJ/g)	E_2 (kJ/g)	E_3 (kJ/g)
zigzag@(9,0)CNT	2.02	0.98	1.99	1.328	0.004	-0.349
armchair@(5,5)CNT	2.04	1.41	2.87	1.555	0.012	-0.161
ZZ1'@(9,0)CNT	2.10	1.88	3.95	1.878	0.038	-0.031
ZZ1'@(8,0)CNT	2.16	2.68	5.80	2.090	0.122	0.469
AC3@(5,5)CNT	2.37	7.46	17.68	5.267	0.787	1.405
ZZ4@(9,0)CNT	2.38	7.49	17.78	5.382	0.781	1.322
ZZ4@(10,0)CNT	2.40	5.34	12.80	4.654	0.204	0.482
TNT	1.64	4.30	7.05			

IX. Coordinates for several of the typical structures

Here we present the coordinates for three typical structures of polymeric nitrogen optimized in corresponding implicit carbon nanotubes ZZ1'@(9,0)ICNT (data_1), AC3@ (5,5)ICNT (data_2) and ZZ4@(10, 0)ICNT (data_3). The coordinates for three additional nitrogen structures displayed above 2ZZ1' @(10, 0)ICNT (data_4), ZZ4' @ (11, 0)ICNT (data_5) and 3eAC@(6, 6)ICNT (data_6) are also provided.

```
data_1


_chemical_name_common                  'N                                        '
_cell_length_a                         15.00000
_cell_length_b                         15.00000
_cell_length_c                         4.38340
_cell_angle_alpha                      90
_cell_angle_beta                       90
_cell_angle_gamma                      90
_space_group_name_H-M_alt              'P 1'
_space_group_IT_number                 1

loop_
_space_group_symop_operation_xyz
   'x, y, z'

loop_
   _atom_site_label
   _atom_site_occupancy
   _atom_site_fract_x
   _atom_site_fract_y
   _atom_site_fract_z
   _atom_site_adp_type
   _atom_site_B_iso_or_equiv
   _atom_site_type_symbol
   N1         1.0     0.501116      0.567202      0.649018     Biso  1.000000 N
   N2         1.0     0.501116      0.567201      0.345432     Biso  1.000000 N
   N3         1.0     0.500285      0.427548      0.497237     Biso  1.000000 N
   N4         1.0     0.496685      0.440208      0.997233     Biso  1.000000 N
   N5         1.0     0.500142      0.482500      0.732849     Biso  1.000000 N
   N6         1.0     0.500142      0.482496      0.261617     Biso  1.000000 N
```

data_2

_chemical_name_common	'N '
_cell_length_a	15.00000
_cell_length_b	15.00000
_cell_length_c	3.83403
_cell_angle_alpha	90
_cell_angle_beta	90
_cell_angle_gamma	90
_space_group_name_H-M_alt	'P 1'
_space_group_IT_number	1

loop_
_space_group_symop_operation_xyz
'x, y, z'

loop_
_atom_site_label
_atom_site_occupancy
_atom_site_fract_x
_atom_site_fract_y
_atom_site_fract_z
_atom_site_adp_type
_atom_site_B_iso_or_equiv
_atom_site_type_symbol

N1	1.0	0.414851	0.498548	0.055927	Biso	1.000000	N
N2	1.0	0.414851	0.498548	0.444073	Biso	1.000000	N
N3	1.0	0.541330	0.574461	0.055917	Biso	1.000000	N
N4	1.0	0.541330	0.574461	0.444083	Biso	1.000000	N
N5	1.0	0.458674	0.425524	0.944081	Biso	1.000000	N
N6	1.0	0.585152	0.501436	0.944073	Biso	1.000000	N
N7	1.0	0.543831	0.426967	0.055921	Biso	1.000000	N
N8	1.0	0.456171	0.573018	0.944080	Biso	1.000000	N
N9	1.0	0.543831	0.426967	0.444079	Biso	1.000000	N
N10	1.0	0.456171	0.573018	0.555920	Biso	1.000000	N
N11	1.0	0.458674	0.425524	0.555919	Biso	1.000000	N
N12	1.0	0.585152	0.501436	0.555927	Biso	1.000000	N

data_3

```
_chemical_name_common                  'N                                       '
_cell_length_a                         15.00000
_cell_length_b                         15.00000
_cell_length_c                         2.27347
_cell_angle_alpha                      90
_cell_angle_beta                       90
_cell_angle_gamma                      90
_space_group_name_H-M_alt              'P 1'
_space_group_IT_number                 1

loop_
_space_group_symop_operation_xyz
   'x, y, z'

loop_
   _atom_site_label
   _atom_site_occupancy
   _atom_site_fract_x
   _atom_site_fract_y
   _atom_site_fract_z
   _atom_site_adp_type
   _atom_site_B_iso_or_equiv
   _atom_site_type_symbol
   N1         1.0     0.596085      0.474107      0.500000     Biso  1.000000 N
   N2         1.0     0.403915      0.525893      0.500000     Biso  1.000000 N
   N3         1.0     0.525894      0.596086      0.000000     Biso  1.000000 N
   N4         1.0     0.474106      0.403914      1.000000     Biso  1.000000 N
   N5         1.0     0.403914      0.474106      1.000000     Biso  1.000000 N
   N6         1.0     0.596086      0.525894     -0.000000     Biso  1.000000 N
   N7         1.0     0.474107      0.596085      0.500000     Biso  1.000000 N
   N8         1.0     0.525893      0.403915      0.500000     Biso  1.000000 N
```

```
data_4

_chemical_name_common                  'N                                   '
_cell_length_a                         20.00000
_cell_length_b                         20.00000
_cell_length_c                         4.37808
_cell_angle_alpha                      90
_cell_angle_beta                       90
_cell_angle_gamma                      90
_space_group_name_H-M_alt              'P 1'
_space_group_IT_number                 1

loop_
_space_group_symop_operation_xyz
   'x, y, z'

loop_
   _atom_site_label
   _atom_site_occupancy
   _atom_site_fract_x
   _atom_site_fract_y
   _atom_site_fract_z
   _atom_site_adp_type
   _atom_site_B_iso_or_equiv
   _atom_site_type_symbol
   N1         1.0     0.559532      0.518421      0.736309     Biso  1.000000 N
   N2         1.0     0.440468      0.481579      0.263691     Biso  1.000000 N
   N3         1.0     0.440468      0.481579      0.736309     Biso  1.000000 N
   N4         1.0     0.559532      0.518421      0.263691     Biso  1.000000 N
   N5         1.0     0.562613      0.454330      0.650007     Biso  1.000000 N
   N6         1.0     0.437387      0.545670      0.349993     Biso  1.000000 N
   N7         1.0     0.437387      0.545670      0.650007     Biso  1.000000 N
   N8         1.0     0.562613      0.454330      0.349993     Biso  1.000000 N
   N9         1.0     0.443886      0.440807      0.500000     Biso  1.000000 N
   N10        1.0     0.556114      0.559193      0.500000     Biso  1.000000 N
   N11        1.0     0.456105      0.452007     -0.000000     Biso  1.000000 N
   N12        1.0     0.543895      0.547993      0.000000     Biso  1.000000 N
```

data_5

_chemical_name_common ’N ’
_cell_length_a 20.00000
_cell_length_b 20.00000
_cell_length_c 4.48880
_cell_angle_alpha 90
_cell_angle_beta 90
_cell_angle_gamma 90
_space_group_name_H-M_alt ’P 1’
_space_group_IT_number 1

loop_
_space_group_symop_operation_xyz
’x, y, z’

loop_
_atom_site_label
_atom_site_occupancy
_atom_site_fract_x
_atom_site_fract_y
_atom_site_fract_z
_atom_site_adp_type
_atom_site_B_iso_or_equiv
_atom_site_type_symbol

N1	1.0	0.547847	0.582274	0.583549	Biso	1.000000	N
N2	1.0	0.452152	0.417728	0.083552	Biso	1.000000	N
N3	1.0	0.417729	0.547848	0.333554	Biso	1.000000	N
N4	1.0	0.582272	0.452154	0.833547	Biso	1.000000	N
N5	1.0	0.442904	0.576163	0.568438	Biso	1.000000	N
N6	1.0	0.557098	0.423839	0.068435	Biso	1.000000	N
N7	1.0	0.423838	0.442902	0.318439	Biso	1.000000	N
N8	1.0	0.576162	0.557099	0.818441	Biso	1.000000	N
N9	1.0	0.452669	0.422227	0.566795	Biso	1.000000	N
N10	1.0	0.547333	0.577774	0.066789	Biso	1.000000	N
N11	1.0	0.577772	0.452670	0.316791	Biso	1.000000	N
N12	1.0	0.422230	0.547330	0.816794	Biso	1.000000	N
N13	1.0	0.555981	0.428351	0.585191	Biso	1.000000	N
N14	1.0	0.444021	0.571651	0.085194	Biso	1.000000	N
N15	1.0	0.571651	0.555980	0.335190	Biso	1.000000	N
N16	1.0	0.428349	0.444019	0.835193	Biso	1.000000	N
N17	1.0	0.387346	0.493428	0.825989	Biso	1.000000	N
N18	1.0	0.612654	0.506575	0.325986	Biso	1.000000	N

```
   N19         1.0      0.506573      0.387346      0.575986     Biso  1.000000 N
   N20         1.0      0.493427      0.612657      0.075986     Biso  1.000000 N
```

data_6

```
_chemical_name_common                  'N                                   '
_cell_length_a                         20.00000
_cell_length_b                         20.00000
_cell_length_c                         8.15994
_cell_angle_alpha                      90
_cell_angle_beta                       90
_cell_angle_gamma                      90
_space_group_name_H-M_alt              'P 1'
_space_group_IT_number                 1

loop_
_space_group_symop_operation_xyz
   'x, y, z'

loop_
   _atom_site_label
   _atom_site_occupancy
   _atom_site_fract_x
   _atom_site_fract_y
   _atom_site_fract_z
   _atom_site_adp_type
   _atom_site_B_iso_or_equiv
   _atom_site_type_symbol
   N1          1.0      0.578630      0.515645      0.172922     Biso  1.000000 N
   N2          1.0      0.515652      0.578640      0.827077     Biso  1.000000 N
   N3          1.0      0.515653      0.578639      0.672922     Biso  1.000000 N
   N4          1.0      0.578629      0.515647      0.327081     Biso  1.000000 N
   N5          1.0      0.423852      0.513669      0.077568     Biso  1.000000 N
   N6          1.0      0.513675      0.423841      0.922431     Biso  1.000000 N
   N7          1.0      0.513674      0.423840      0.577575     Biso  1.000000 N
   N8          1.0      0.423851      0.513669      0.422425     Biso  1.000000 N
   N9          1.0      0.560245      0.447252      0.672865     Biso  1.000000 N
   N10         1.0      0.447252      0.560251      0.327122     Biso  1.000000 N
   N11         1.0      0.447253      0.560253      0.172879     Biso  1.000000 N
   N12         1.0      0.560246      0.447253      0.827135     Biso  1.000000 N
```

N13	1.0	0.427427	0.526152	0.577556	Biso	1.000000 N
N14	1.0	0.526155	0.427429	0.422445	Biso	1.000000 N
N15	1.0	0.526154	0.427429	0.077555	Biso	1.000000 N
N16	1.0	0.427427	0.526151	0.922444	Biso	1.000000 N
N17	1.0	0.474115	0.424027	0.172856	Biso	1.000000 N
N18	1.0	0.424036	0.474108	0.827137	Biso	1.000000 N
N19	1.0	0.424036	0.474109	0.672857	Biso	1.000000 N
N20	1.0	0.474116	0.424027	0.327148	Biso	1.000000 N
N21	1.0	0.549876	0.559070	0.077559	Biso	1.000000 N
N22	1.0	0.559064	0.549863	0.922442	Biso	1.000000 N
N23	1.0	0.559065	0.549863	0.577562	Biso	1.000000 N
N24	1.0	0.549875	0.559071	0.422437	Biso	1.000000 N

References

[1] Chen J, Schusteritsch G, Pickard C J, Salzmann C G and Michaelides A 2016 *Phys. Rev. Lett.* **116** 025501.

[2] Grimme S, Antony J, Ehrlich S and Krieg H 2010 *The Journal of Chemical Physics* **132** 154104.

[3] Klimeš J, Bowler D R and Michaelides A 2009 *Journal of Physics: Condensed Matter* **22** 022201.

[4] Zhang J, Oganov A R, Li X and Niu H 2017 *Physical Review B* **95** 020103.